## Supporting Information

# Photosensitive polyoxometalate-induced formation of thermotropic liquid crystal nanomaterial and its photovoltaic effect

Jian-Sheng Li,‡[a] Xiao-Jing Sang,‡[a] Wei-Lin Chen,*[a] Rong-Lin Zhong,[a] Ying Lu,*[a] Lan-Cui Zhang,[b] Zhong-Min Su,[a] and En-Bo Wang*[a]

[a] *Key Laboratory of Polyoxometalate Science of Ministry of Education, Faculty of Chemistry, Northeast Normal University, Changchun, Jilin 130024, People's Republic of China*

[b] *School of Chemistry and Chemical Engineering, Liaoning Normal University, Dalian 116029.*

**CONTENTS:**

## I. Experimental Section

### 1. Materials and Methods

$[(CH_3)_4N]_5[PW_{11}O_{39}RhCH_2CO_2H]\cdot xH_2O$ was synthesized according to the similar literature method[S1] and characterized by FTIR. Dimethyldioctadecylammonium chloride (DODACl), Tetraheptylammonium bromide ($[CH_3(CH_2)_6]_4NBr$) and all other chemical reagents were commercially purchased and used without further purification. FTIR spectra were recorded in the range 400-4000 $cm^{-1}$ on an Agilent Technologies Cary 630 FTIR Spectrophotometer. Thermogravimetric (TG) analyses were performed on a Perkin-Elmer TGA7 instrument in flowing $N_2$ with a heating rate of $10^oC\ min^{-1}$. $^1H$ NMR spectra were performed on Bruker-DPX 300 NMR spectroscopy. DSC measurements were performed on a Netzsch DSC 204, and the samples were sealed in aluminum capsules in air, and the holder atmosphere was dry nitrogen. The optical textures were observed using a polarizing optical microscope (XP-400E, China) with a hot stage. For VT-XRD measurements, a Bruker AXS D8 ADVANCE X-ray diffractometer using Cu *K*α radiation of a wavelength of 1.54Å and an mri Physikalische Geräte GmbH TC-Basic temperature chamber was used. HRTEM observations were carried out using a JEM-2100F microscope with an accelerating voltage of 200 kV. Cyclic voltammograms were recorded using a three electrode system comprising of glassy carbon electrode as the working electrode, a Pt wire as the counter electrode and Ag/AgCl reference electrode. The surface photovoltage spectroscopy measurement is carried out on a lab-made instrument, which constitutes a source of monochromatic light, a lock-in amplifier (SR830-DSP) with a light chopper (SR540) and a photovoltaic cell. A 500 W xenon lamp (CHFXQ500 W, Global xenon lamp power) and a double-prism monochromator (Hilger and Watts, D300) provides monochromatic light. The construction of the photovoltaic cell was a sandwich-like structure of ITO-sample-ITO. All of the calculations were performed with the Gaussian 09 program package.[S2]

### 2. Synthesis

**Synthesis of $K_7[PW_{11}O_{39}]\cdot xH_2O$**: 72.5 g (0.22 mol) $Na_2WO_4\cdot 2H_2O$ and 7.16 g $Na_2HPO_4\cdot 12H_2O$ (0.02 mol) were dissolved in 100 mL water, which was heated to

70-80 °C. $HNO_3$ was added to adjust the pH of the solution to 3.0. The solution was then heated at 80 °C and concentrated to half of the initial volume. Addition of 10 g KCl and storage at 4 °C for a while resulted in the final product (~40 g).

**Synthesis of $[(CH_3)_4N]_5[PW_{11}O_{39}RhCH_2CO_2H]\cdot xH_2O$**: 4.0 g (1.22 mmol) of $\{PW_{11}\}$ was dissolved in 40 mL of a 0.5 M sodium acetate buffer solution (pH 4.0) to form solution A. 0.35 g (1.32 mmol) of $RhCl_3\cdot xH_2O$ was dissolved in 12 mL water to form solution B, which was added dropwise to solution A with stirring. Then the mixed solution was transferred to the stainless steel kettle and heated to 120 °C for 17 h. 2 g of KCl was added, followed by freeze for 1 h. After filtering out the green precipitation, 1 g of $(CH_3)_4NCl$ was added to the dark red solution. Finally, the orange precipitate could be obtained and washed with 2:1 (v/v) water-ethanol mixture.

**Synthesis of $[DODA]_5[PW_{11}O_{39}RhCH_2CO_2H]\cdot 28H_2O$ (1)**: compound **1** was synthesized according to a similar literature method.[S3] Specifically, a chloroform solution of DODACl was added dropwise to the aqueous solution of $\{PW_{11}Rh\}$ with stirring gently. The molar ratio of DODACl and $\{PW_{11}Rh\}$ was controlled at 5:1. The color of the organic phase changed to orange in several minutes. After stirring gently for 4h at room temperature, the organic phase was separated and evaporated to dryness. The target product was orange powder, which was further dried under vacuum. The FTIR spectra of **1** was shown in Figure S1. $^1H$ NMR spectra in Figure S2 was further employed to characterize the chemical component of **1**. According to the TG analysis (Figure S3) and the charge balance consideration, the chemical formula of **1** should be $[DODA]_5[PW_{11}O_{39}RhCH_2CO_2H]\cdot 28H_2O$.

**Synthesis of $\{[CH_3(CH_2)_6]_4N\}_5[PW_{11}O_{39}RhCH_2COOH]\cdot 6H_2O$ (2)**: the synthetic procedure above was followed using $[CH_3(CH_2)_6]_4NBr$ instead of DODACl. The obtained product presented a viscous state. The FTIR spectra of **2** was shown in Figure S4. $^1H$ NMR spectra in Figure S5 was further employed to characterize the chemical component of **2**. According to the TG analysis (Figure S6) and the charge balance consideration, the chemical formula of **2** should be $\{[CH_3(CH_2)_6]_4N\}_5[PW_{11}O_{39}RhCH_2COOH]\cdot 6H_2O$.

**II. Supplementary Physical and Chemical Characterizations**

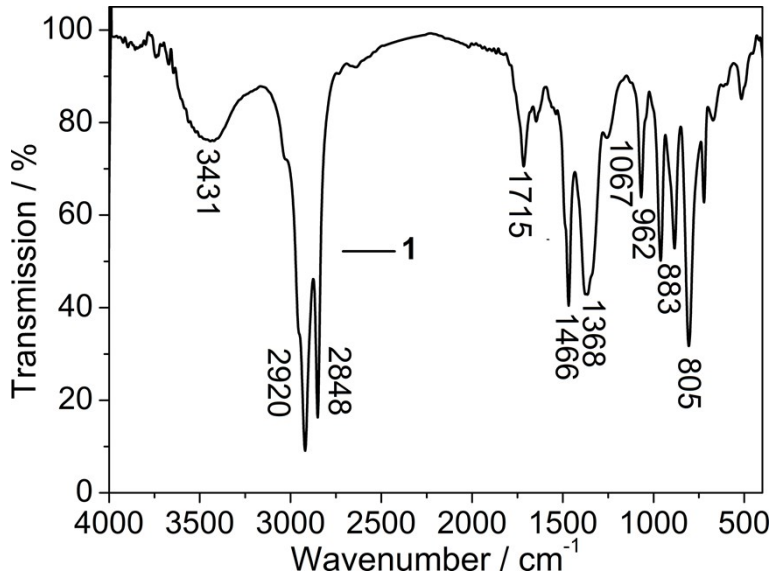


Figure S1. FTIR spectra of compound **1**

As shown in Figures S1, the wide band centering at 3431 $cm^{-1}$ are attributed to $\nu$(O-H) vibration of water molecules. The peaks at 2920 and 2848 $cm^{-1}$ are attributed to the asymmetric stretching ($\nu_{as}$) and symmetric stretching ($\nu_{s}$) vibration of the organic group $–CH_2$. The peak at 1715 $cm^{-1}$ are assigned to the stretching vibration of the group of –COOH. The peaks located at 1466 and 1368 $cm^{-1}$ are ascribed to the vibration of $–CH_2$ and $–CH_3$ respectively. The characteristic vibrations of $\nu(P–O_a)$, $\nu(W–O_d)$, $\nu(W–O_b–W)$ and $\nu(W–O_c–W)$ of POM anions appear at 1067, 962, 883 and 805 $cm^{-1}$ respectively ($O_d$, terminal O atoms; $O_b$, $O_c$, bridging O atoms). The results indicated that compound **1** was constituted of $DODA^+$ and POM anion.

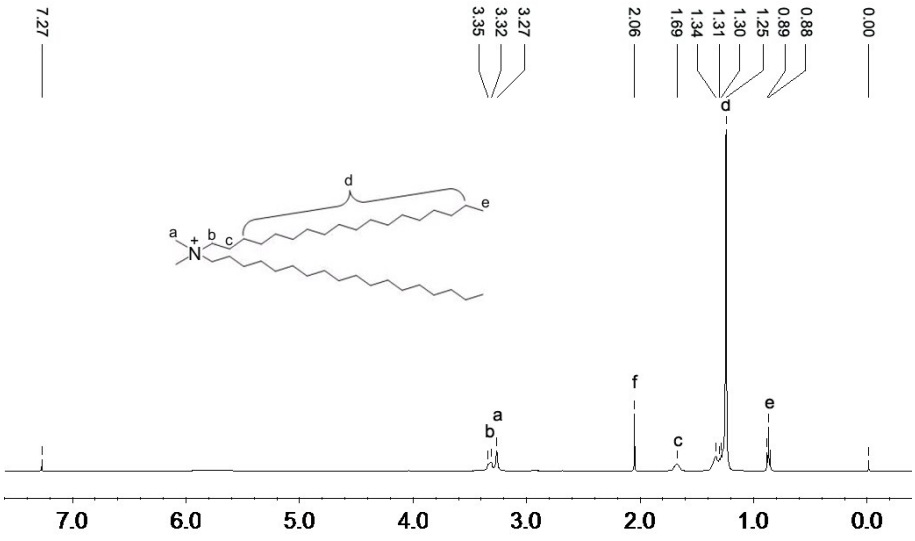

Figure S2. $^1$H NMR spectra in $CD_3Cl$ of compound **1**

The $^1$H NMR spectra was employed to characterize the chemical structure of **1**. As shown in Fig. S2, a six-line pattern in the $^1$H NMR spectra for compound **1** was observed. From the inset of Fig. S2, different kinds of H atoms in $DODA^+$ were denoted as $a_H$, $b_H$, $c_H$, $d_H$ and $e_H$, due to which the chemical shifts of the peaks were located at 3.27, 3.32 (3.35), 1.69, 1.25 (1.30, 1.31, 1.34) and 0.88 (0.89) ppm. The chemical shift of the peak at 2.06 ppm was assigned to H atoms of the group $–CH_2$ in $\{PW_{11}Rh\}$. The results indicated that compound **1** was composed of $\{PW_{11}Rh\}$ anion and $DODA^+$, which was consistent with the result of FTIR.

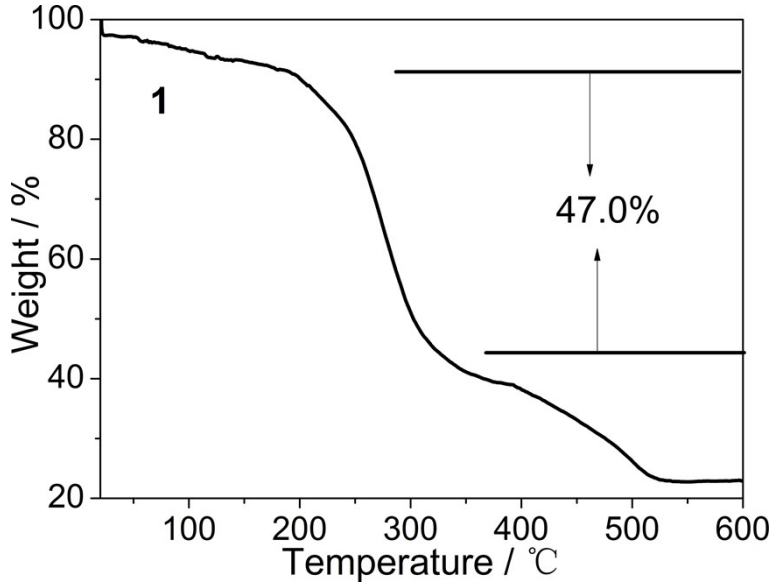


Figure S3. TG curve of compound **1**

The TG curve of **1** in Figure S3 shows the first weight loss step of 8.8% (calc. 8.26%) in the range of 20-190 °C, which corresponds to the loss of water molecules. The second weightloss of 47.0% (calc. 45.2%) in the range of 190-326 °C was corresponding to the loss of five $DODA^+$ groups. Further temperature increment lead to continuous weightloss, indicating that the skeleton of POMs decomposed.

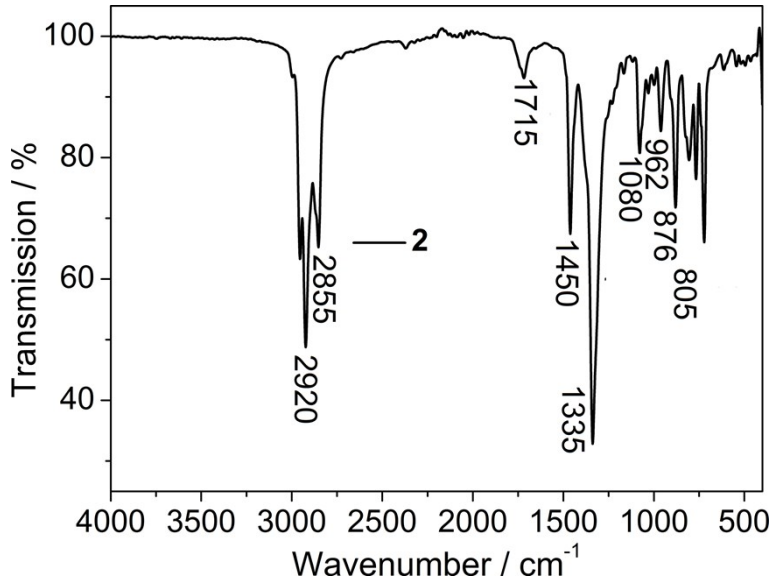


Figure S4. FTIR spectra of compound **2**

The characteristic peaks of FTIR spectra for compound **2** was similar with that of **1**. As shown in Fig. S4, the peaks at 2920 and 2855 $cm^{-1}$ are attributed to the $\nu_{as}$ and $\nu_{s}$ vibration of the organic group $–CH_2$. The peak located at 1715 $cm^{-1}$ is assigned to the stretching vibration of the group of –COOH. The peaks at 1450 and 1335 $cm^{-1}$ are ascribed to the vibration of $–CH_2$ and $–CH_3$ respectively. The characteristic vibrations of $\nu(P–O_a)$, $\nu(W–O_d)$, $\nu(W–O_b–W)$ and $\nu(W–O_c–W)$ of POM anions appear at 1080, 962, 876 and 805 $cm^{-1}$ respectively. The results indicated that **2** was composed of $DODA^+$ and POM anion.

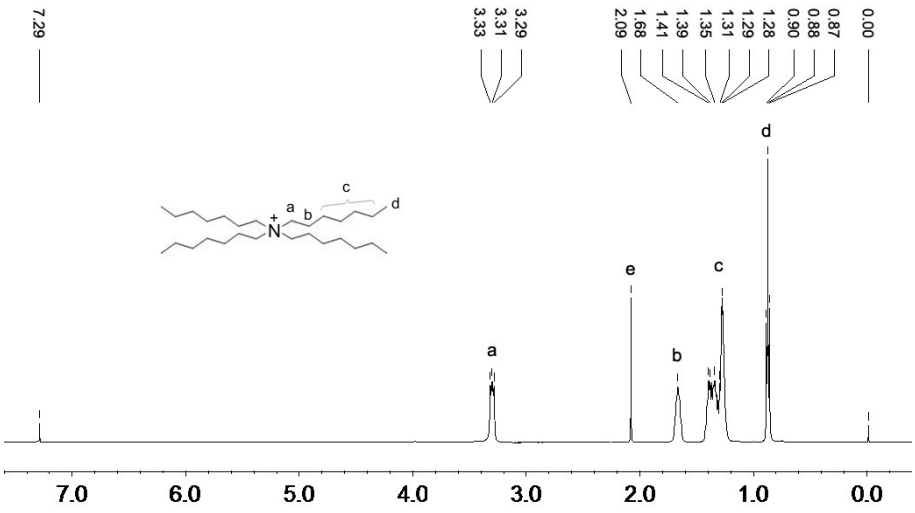


Figure S5. $^{1}$H NMR of compound **2**

The $^{1}$H NMR spectra was further performed to characterize the chemical structure of **2**. As can be seen in Fig. S5, a five-line pattern in the $^{1}$H NMR spectra for **2** was observed. Different kinds of H atoms in $[CH_3(CH_2)_6]_4N^+$ were denoted as $a_H$, $b_H$, $c_H$ and $d_H$ in the inset of Fig. S5, and their chemical shifts were located at 3.29 (3.31, 3.33), 1.68, 1.28 (1.29, 1.31, 1.35, 1.39, 1.41) and 0.87 (0.88, 0.90) ppm. The chemical shift of the peak at 2.09 ppm was assigned to H atoms of the group $–CH_2$ in $\{PW_{11}Rh\}$. The results indicated that compound **2** was composed of $\{PW_{11}Rh\}$ anion and $DODA^+$, which was consistent with the result of FTIR.

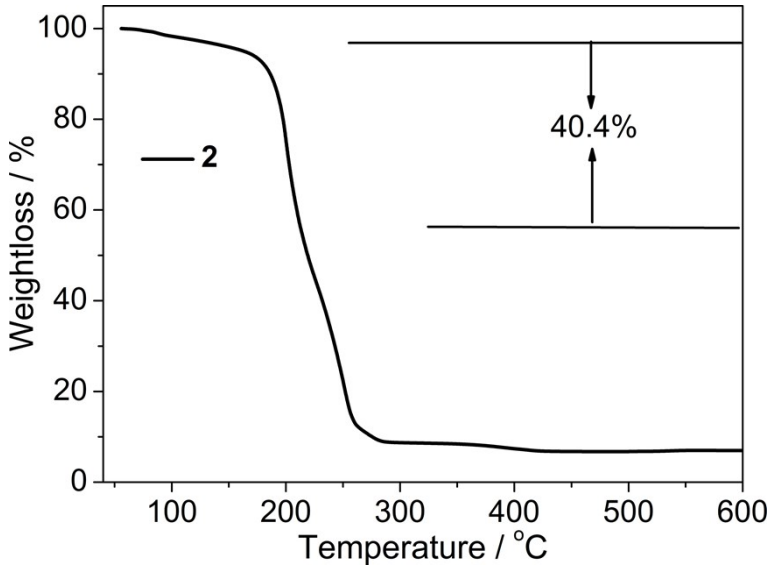


Figure S6. TG curve of compound **2**

The TG curve of **2** in Figure S3 shows the first weightloss step of 3.5% (calc. 3.4%)

in the range of 40-142 °C, which was ascribed to the loss of water molecules. The second weightloss of 40.4% (calc. 41.1%) in the range of 142-213 °C was attributed to the loss of five $[CH_3(CH_2)_6]_4N^+$ groups. Further temperature increment resulted in the degradation of the skeleton of POMs.

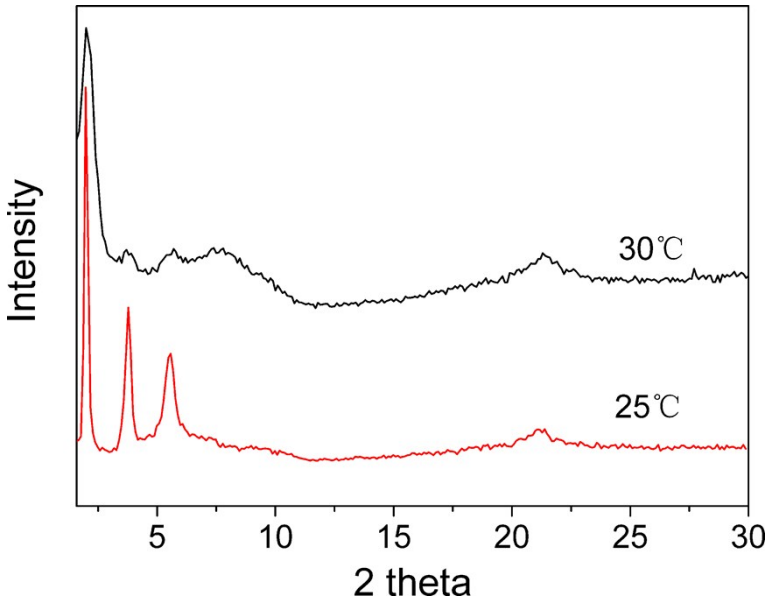


Fig. S7. VT-XRD patterns of **1** at 25 °C (red line) and 30 °C (dark line).

As can be seen from Fig. S7, the VT-XRD of compound **1** at 25 °C contained three equidistant peaks at small angles which confirmed the formation of a layer structure in its solid state. Additionally, the distance of the two neighboring layers was calculated to be 4.46nm from the Bragg equation, which was slightly different from that of of 4.41 nm at 30 °C, which indicated that the transitions between different phases of the solid state occurred at 28.6 °C corresponding to the second peak during the second heating process.

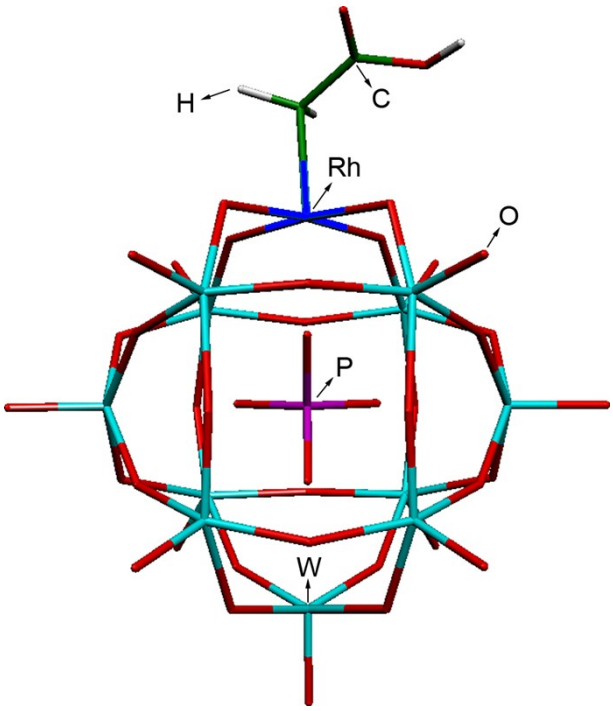


Figure S8. The optimized structure of $[PW_{11}O_{39}RhCH_2CO_2H]^{5-}$

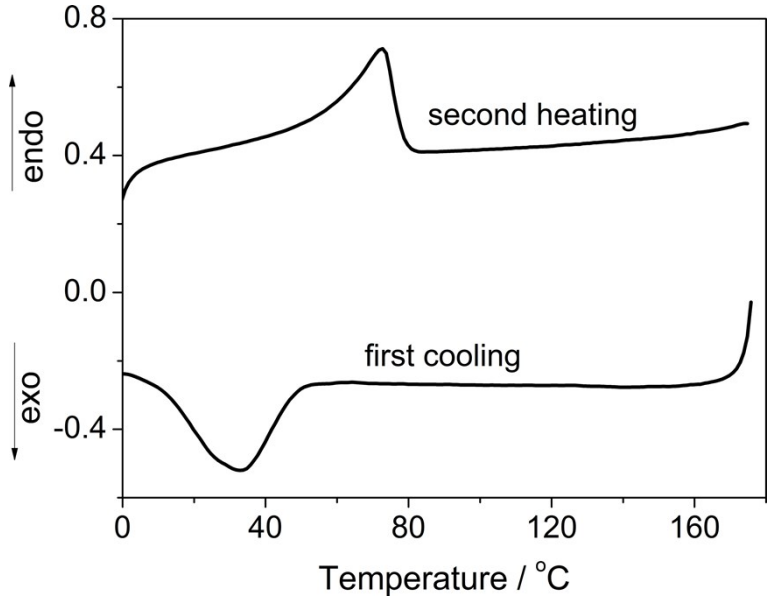


Figure S9. DSC curve of compound **2** for its first cooling and second heating processes

As shown in Fig. S9, for **2**, upon the second heating process, a peak at 73 °C could be clearly observed, which corresponds to the phase transition between the solid state to the isotropic phase. During the first cooling run, the phase transition between the isotropic phase to the solid state occurred at 34 °C. The result indicated that **2** can be regarded as a kind of POM-based ionic liquid.

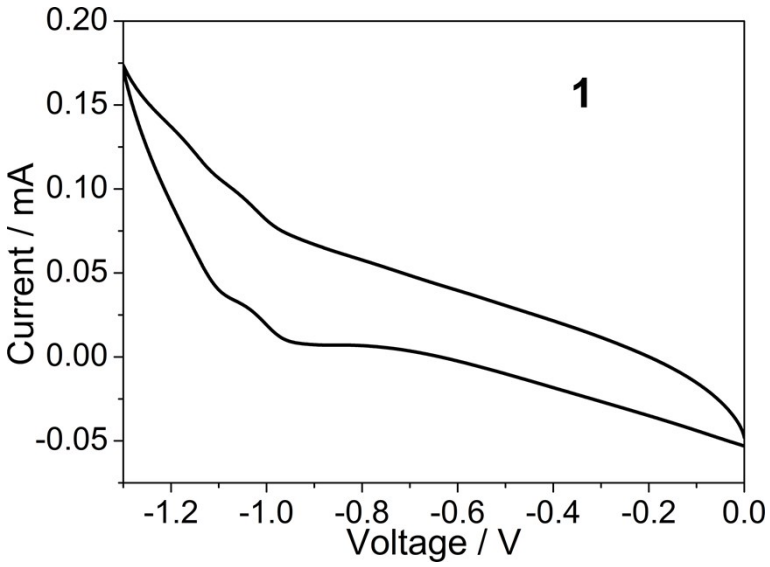


Figure S10. Cyclic voltammograms of compound **1** in 0.5M NaAc/HAc buffer solution with pH 4.0

The electrochemical properties of compound **1** was investigated through the cyclic voltammetric method in Fig. S10, which was recorded in the three electrode system consisting of the **1**-doped carbon paste electrode as the working electrode, a Pt wire as the counter electrode and Ag/AgCl as the reference electrode. As shown Fig. S10, there are two cathodic peaks located at -1.05 V and -1.18 V, which are accompanied by two anodic peaks at -0.95 V and -1.09 V respectively, corresponding to the reduction and oxidation processes of W centers in $\{PW_{11}Rh\}$ anion. This phenomenon indicated that **1** possesses excellent redox properties.

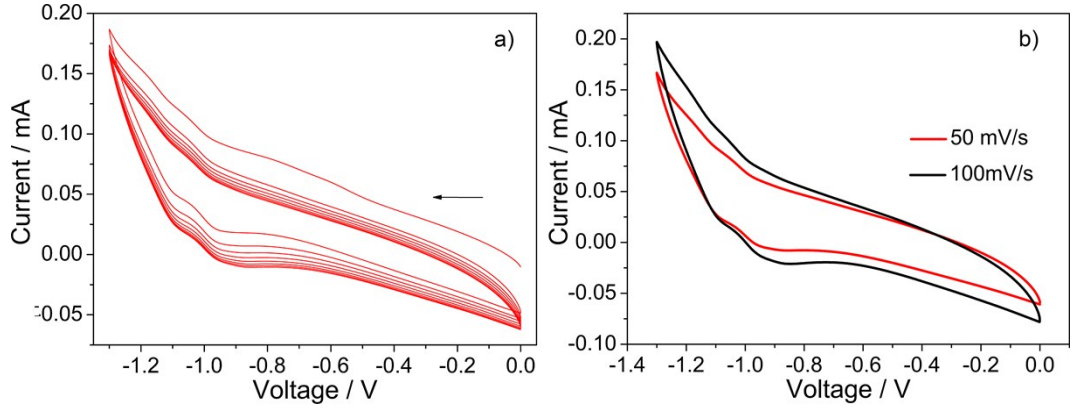


Fig. S11. (a) CV curves of compound **1** in 0.5M NaAc/HAc buffer solution with pH 4.0 at the scanning rate of 50 mV/s; (b) CV curves of compound **1** at different scanning rates.

To check the reproducibility of the cyclic voltamograms (CV), the electrochemical

properties of compound **1** was retested and the CV curves were recorded by scanning eight cycles. As can be seen from Fig. S11a, the positions of the cathodic peaks and anodic peaks remained almost the same. Meanwhile, the CV curves at different scanning rates were obtained, which indicated that the reproducibility of the cyclic voltamograms is good.

**III. Table**

Table S1. The phase transition temperatures, enthalpies and assignments of the phase transition for compound **1** and **2** (S1 = solid 1, S2 = solid 2, S3 = solid 3, SmA = smectic A, Iso = isotropic phase) on the second heating process.

| Compound | Transition | Temperature / $^{o}$C | $\Delta$H / kJ mol$^{-1}$ |
|---|---|---|---|
| **1** | S1-S2 | 22 | 4.49 |
| | S2-S3 | 29 | 2.77 |
| | S3-SmA | 36 | 4.92 |
| **2** | S1-Iso | 73 | 25.64 |

References:

S1 X. Y. Wei, M. H. Dickman, and M. T. Pope, *J. Am. Chem. Soc.*, 1998, 120, 10254-10255.

S2 M. J. Frisch, G. W. Trucks, H. B. Schlegel, G. E. Scuseria, M. A. Robb, J. R. Cheeseman, J. A. Montgomery, T. Vreven, K. N. Kudin, J. C. Burant, J. M. Millam, S. S. Iyengar, J. Tomasi, V. Barone, B. Mennucci, M. Cossi, G. Scalmani, N. Rega, G. A. Petersson, H. Nakatsuji, M. Hada, M. Ehara, K. Toyota, R. Fukuda, J. Hasegawa, M. Ishida, T. Nakajima, Y. Honda, O. Kitao, H. Nakai, M. Klene, X. Li, J. E. Knox, H. P. Hratchian, J. B. Cross, V. Bakken, C. Adamo, J. Jaramillo, R. Gomperts, R. E. Stratmann, O. Yazyev, A. J. Austin, R. Cammi, C. Pomelli, J. W. Ochterski, P. Y. Ayala, K. Morokuma, G. A. Voth, P. Salvador, J. J. Dannenberg, V. G. Zakrzewski, S. Dapprich, A. D. Daniels, M. C. Strain, O. Farkas, D. K. Malick, A. D. Rabuck, K. Raghavachari, J. B. Foresman, J. V. Ortiz, Q. Cui, A. G. Baboul, S. Clifford, J. Cioslowski, B. B. Stefanov, G. Liu, A. Liashenko, P. Piskorz, I. Komaromi, R. L. Martin, D. J. Fox, T. Keith, M. A. Al-Laham, C. Y. Peng, A. Nanayakkara, M.

Challacombe, P. M. W. Gill, B. Johnson, W. Chen, M. W. Wong, C. Gonzalez and J. A. Pople , *Gaussian 09, Revision A.02*, Gaussian, Inc, Wallingford, CT, 2009.

S3 D. Volkmer, A. D. Chesne, D. G. Kurth, H. Schnablegger, P. Lehmann, M. J. Koop, and A. Müller, *J. Am. Chem. Soc.*, 2000, **122**, 1995-1998.